Interfaces and Free Boundaries **3**, (2001) 393–414

Numerical diffusion-induced grain boundary motion

K. DECKELNICK, C. M. ELLIOTT AND V. STYLES
Centre for Mathematical Analysis and Its Applications, School of Mathematical Sciences, University of Sussex, Falmer, Brighton BN1 9QH, UK

[Received 1 June 2000 and in revised form 14 December 2000]

In this paper we consider the numerical approximation of phase field and sharp interface models for diffusion-induced grain boundary motion. The phase field model consists of a double-obstacle Allen–Cahn equation with a forcing obtained from the solution of a degenerate diffusion equation. On the other hand the sharp interface model consists of forced mean curvature flow coupled to a diffusion equation holding on the interface itself. Formal asymptotics yield the sharp interface model as the limit of the phase field equations as the width of the associated diffuse interface tends to zero. A finite-element approximation of the phase field model is presented and is shown to be convergent to a weak solution. Numerical simulations of both models are described and compared. It is shown that the two models are consistent.

Keywords: Grain boundary motion; phase field model; sharp interface; mean curvature flow; finite-element approximation.

1. Introduction

If a thin polycrystalline film of a metal is placed in a vapour containing another metal, then atoms from the vapour diffuse into the film along the grain boundaries separating the crystals. The boundaries are observed to move with one of the abutting grains growing and one shrinking. This motion is known as diffusion-induced grain boundary motion (DIGM). The newly created crystal that is produced behind the advancing grain is different from that in front as it has metal diffused from the vapour deposited in it [12, 15, 16]. In [5] the following phase field model for DIGM with a diffuse interface of finite thickness $\mathrm{O}(\varepsilon)$ is presented along with a theoretical framework for exploring the driving forces behind the motion:

$$\rho\varphi_t - \Delta\varphi - \frac{1}{\varepsilon^2}\varphi + \beta(\varphi) + \frac{P_\varphi(u,\varphi)}{\varepsilon} \ni 0 \quad \text{in} \quad \Omega_{\mathrm{T}} = \Omega \times (0,T), \tag{1.1}$$

and

$$\varepsilon u_t = \nabla \cdot (D(\varphi)\nabla w) \quad \text{in} \quad \Omega_{\mathrm{T}}. \tag{1.2}$$

The above model uses two dimensionless field variables, u and φ. The variable u, lying in the range $0 \leqslant u \leqslant 1$, represents the concentration of solute atoms in the film. The other variable φ is an order parameter lying in the range $-1 \leqslant \varphi \leqslant 1$, which distinguishes the two crystals, taking the value $+1$ on one side of the grain boundary between the two perfectly crystalline grains, -1 on the other side, and intermediate values in the grain boundary itself. The geometrical configuration is that of a film with a rectangular cross section $\Omega \subset \mathbb{R}^2$ such that $\mathbf{x} \in \Omega = (-H, H) \times (-L, L)$ and $t \in (0, T)$ is time, for which there is a grain boundary that spans the width of the film. We may think of the

diffuse grain boundary $\Omega_\Gamma(t)$ in which $|\varphi| < 1$ as some kind of mixture of the two crystals, in the proportions $1+\varphi : 1-\varphi$.

In this model there is a homogeneous free energy $P(u,\varphi) + \frac{W(\varphi)}{\varepsilon}$ where $W(\varphi)$ is the classical double obstacle potential [3] and

$$P(u,\varphi) = q(\varphi) f(u)$$

for appropriate non-negative functions q and f with $f(0) = 0$. The use of W in (1.1) implies that the grain boundary $\Omega_\Gamma(t)$ is of finite thickness $\mathrm{O}(\varepsilon)$. In the diffusion equation (1.2) we have the chemical potential

$$w = u + \frac{\varepsilon}{u^*} P_u(u,\varphi).$$

(The parameters ρ and u^* are given positive, non-dimensional material constants.) The diffusivity coefficient D vanishes outside the grain boundary so that concentration only diffuses within the grain boundary. We are concerned with a DIGM for which the boundary motion is monotone in one direction so that once the diffuse interface passes through a point the concentration at that point then remains unchanged. It follows that ahead of the grain boundary we have the initial crystalline state whereas behind the grain boundary there is a newly formed crystal with a changed composition caused by the diffusion of vapour atoms and behind that crystal there is again the original crystalline state. This is depicted schematically in Fig. 1. In [10] formal asymptotics on the phase field model for $\varepsilon \to 0$ are used to obtain the following sharp interface model:

$$\rho V = \kappa + f(u) \tag{1.3}$$

$$u_{ss} = Vu, \tag{1.4}$$

where V, κ and s are respectively the normal velocity, the curvature and the arc-length of the sharp interface. A modified more accurate problem retaining $\mathrm{O}(\varepsilon)$ terms in (1.4) is

$$\rho V = \kappa + f(u) \tag{1.5}$$

$$\varepsilon_1 u_t = u_{ss} - Vu(1+\varepsilon_2\kappa) = u_{ss} - Vu(1+\varepsilon_2(\rho V - f(u))), \tag{1.6}$$

where $\varepsilon_i = \mathrm{O}(\varepsilon)$, $i = 1, 2$. These equations are in the non-dimensionalized form presented in [10]. The existence of a unique weak solution to one form of the phase field system (1.1), (1.2) was proved in [7] while in [14] a local existence and uniqueness result for (1.5), (1.6) was obtained.

The motivation behind this paper is to justify numerically the connection between the phase field and sharp-interface DIGM models and to illustrate solutions of these two models. Also we want to investigate the long-time behaviour of the two models and to show that in certain parameter ranges their solution converges to travelling waves. The existence of a travelling wave solution to the sharp-interface model was proved in [10]. We compare a simplified form of the phase field model presented in [5] with the sharp-interface model derived in [10] using formal asymptotics. In Section 2 we introduce the phase field and the sharp-interface DIGM models and in the case of the sharp-interface model we present two forms of the model: one using a graph approach presented in [13] and the other using a parametric approach. In Section 3 we derive numerical approximations of the phase field model and the parametric sharp-interface model. Also, for completeness, we include the approximation of the graph sharp-interface model derived in [13]. In Section 4 we prove the convergence of the finite-element phase field approximation. In Section 5 we present numerical computations that compare solutions of the phase field model and the sharp-interface models.

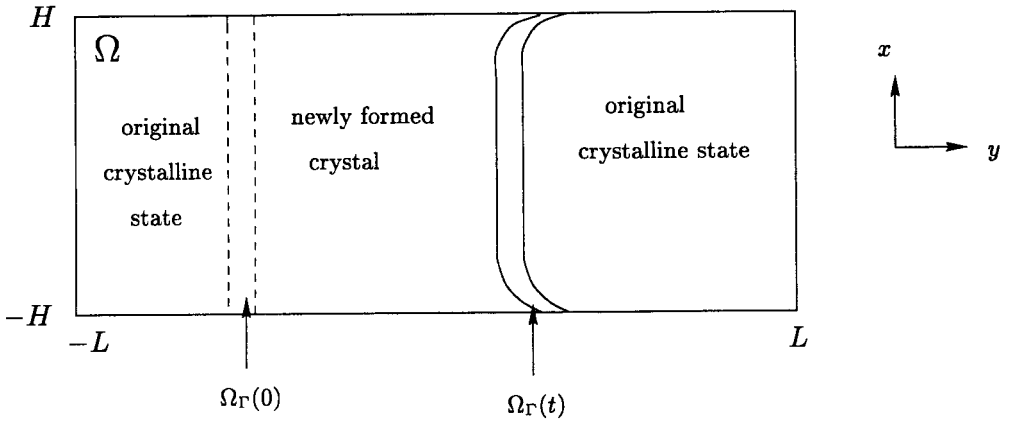

FIG. 1. DIGM.

2. Models

2.1 *Phase field DIGM*

We study the following simplified version of (1.1), (1.2):

$$\rho\varphi_t - \Delta\varphi - \frac{1}{\varepsilon^2}\varphi + \beta(\varphi) + \frac{\pi f(u)}{4\varepsilon} \ni 0 \quad \text{in } \Omega_\Gamma, \tag{2.1}$$

$$\varepsilon u_t = \nabla \cdot (D(\varphi)\nabla u) \quad \text{in } \Omega_\Gamma, \tag{2.2}$$

$$D(\varphi) := \frac{2}{\pi}(1-\varphi^2),$$

where β is the sub-differential of $I_{[-1,1]}$, i.e. $\beta(r) = \partial I_{[-1,1]}(r)$ and

$$I_{[-1,1]}(r) := \begin{cases} 0 & \text{if } r \in [-1,1], \\ +\infty & \text{otherwise.} \end{cases}$$

Thus,

$$\beta(r) = \begin{cases} (-\infty, 0] & \text{if} \quad r = -1, \\ 0 & \text{if} \quad |r| < 1, \\ [0, \infty) & \text{if} \quad r = 1. \end{cases}$$

Note that the constants $\frac{\pi}{4}$ and $\frac{2}{\pi}$ in front of f and D are chosen so that sending $\varepsilon \to 0$ in (2.1), (2.2) yield the sharp-interface equations (1.3), (1.4). We impose the boundary conditions

$$\frac{\partial\varphi}{\partial\nu} = 0, \qquad D(\varphi)\frac{\partial u}{\partial\nu} = \alpha D(\varphi)(1-u) \quad \text{on} \quad \partial\Omega \times (0,T), \tag{2.3}$$

where α is a large positive number. The flux boundary condition (2.3) for the concentration implies that the vapour can only enter the film through the grain boundary. For our initial data we set

$$\varphi(\mathbf{x}, 0) = \varphi_0(\mathbf{x}), \qquad u(\mathbf{x}, 0) = 0 \quad \text{in} \quad \Omega, \tag{2.4}$$

where

$$\varphi_0(x,y) = \begin{cases} -1 & \text{if} \quad y \leqslant -\varepsilon\pi/2, \\ \sin(y/\varepsilon) & \text{if} \quad -\varepsilon\pi/2 < y < \varepsilon\pi/2, \\ 1 & \text{if} \quad y \geqslant \varepsilon\pi/2. \end{cases} \tag{2.5}$$

This initial data corresponds to an initial grain boundary of width $\pi\varepsilon$ across which φ_0 varies monotonically from -1 to $+1$. Furthermore, we assume that initially the concentration of solute atoms in the domain is zero. The problem has been set up so that the grain boundary motion is to the right.

We note that the weak formulation of (2.1), (2.2) is

$$\int_\Omega (\rho(\eta-\varphi)\varphi_t + \nabla\varphi\cdot\nabla(\eta-\varphi)) \geqslant \int_\Omega \left(\frac{\varphi}{\varepsilon^2} - \frac{\pi f(u)}{4\varepsilon}\right)(\eta-\varphi) \quad \forall\, \eta \in K, \tag{2.6}$$

$$\int_\Omega (\varepsilon u_t \xi + D(\varphi)\nabla u\cdot\nabla\xi) = \alpha \int_{\partial\Omega} D(\varphi)(1-u)\xi \quad \forall\, \xi \in H^1(\Omega), \tag{2.7}$$

where

$$K = \{\eta \in H^1(\Omega) : |\eta| \leqslant 1 \text{ in } \Omega\}.$$

2.2 *Sharp-Interface DIGM*

2.2.1 *Graph approach.* In [13] a graph approach was used to study solutions of the sharp-interface model (1.3), (1.4). In particular they considered the sharp-interface Γ_t to be a graph such that

$$\Gamma(t) = \{(x,y) : -H < x < H,\ y = Y(x,t)\}.$$

Adapting this approach to the more complicated model (1.5), (1.6) and noting that $\mathrm{d}s = \sqrt{1+Y_x^2}\,\mathrm{d}x$ where s is the arc-length of Γ, yields the following equations:

$$\frac{\rho Y_t}{\sqrt{1+Y_x^2}} = \frac{\mathrm{d}}{\mathrm{d}x}\left(\frac{Y_x}{\sqrt{1+Y_x^2}}\right) + f(u) \quad -H < x < H,\ t > 0, \tag{2.8}$$

$$\varepsilon_1\sqrt{1+Y_x^2}\,u_t = \frac{\mathrm{d}}{\mathrm{d}x}\left(\frac{1}{\sqrt{1+Y_x^2}}\frac{\mathrm{d}u}{\mathrm{d}x}\right) - Y_t u\left(1+\varepsilon_2\left(\frac{\rho Y_t}{\sqrt{1+Y_x^2}} - f(u)\right)\right) \quad -H < x < H,\ t > 0, \tag{2.9}$$

$$Y(x,0) = 0, \qquad u(x,0) = 0 \qquad -H < x < H, \tag{2.10}$$

$$Y_x(-H,t) = 0, \qquad Y_x(H,t) = 0, \qquad t > 0, \tag{2.11}$$

$$u(-H,t) = u(H,t) = 1 \qquad t > 0. \tag{2.12}$$

2.2.2 *Parametric approach.* Another approach for analysing the motion of an interface $\Gamma(t)$ is to use a parametrization $\mathbf{X}(p,t) = (x(p,t), y(p,t))$ of $\Gamma(t)$, where p is a spatial parameter and t is time. We denote by τ and ν the outward pointing unit tangent and unit normal vectors respectively, with $\tau(p,t) = \frac{\mathbf{X}_p(p,t)}{|\mathbf{X}_p(p,t)|}$ and $\nu(p,t) = \frac{\mathbf{X}_p^\perp(p,t)}{|\mathbf{X}_p(p,t)|}$, where we have set $(\alpha_1,\alpha_2)^\perp = (\alpha_2,-\alpha_1)$. Note

that with s denoting the arc length of the curve we have $\mathrm{d}s = |\mathbf{X}_p|\,\mathrm{d}p$. We arrive at the following system:

$$\mathbf{X} : [0,1] \times [0,T] \longrightarrow \mathbb{R}^2, \quad (p,t) \to \mathbf{X}(p,t), \tag{2.13}$$

$$\rho \mathbf{X}_t = \frac{\mathbf{X}_{pp}}{|\mathbf{X}_p|^2} + f(U)\frac{\mathbf{X}_p^\perp}{|\mathbf{X}_p|}, \tag{2.14}$$

$$\varepsilon_1\, U_t = \frac{1}{|\mathbf{X}_p|}\left(\frac{U_p}{|\mathbf{X}_p|}\right)_p - U\frac{\mathbf{X}_t \cdot \mathbf{X}_p^\perp}{|\mathbf{X}_p|}\left(1 + \varepsilon_2\left(\frac{\rho \mathbf{X}_t \cdot \mathbf{X}_p^\perp}{|\mathbf{X}_p|} - f(U)\right)\right) \tag{2.15}$$

$$\mathbf{X}(p,0) = \mathbf{X}_0(p) = (H(2p-1), 0) \quad U(p,0) = U_0(p) = 0, \tag{2.16}$$

$$x(0,t) = -H, \quad x(1,t) = H, \quad y_p(0,t) = y_p(1,t) = 0, \quad U(0,t) = U(1,t) = 1 \quad t > 0. \tag{2.17}$$

3. Numerical discretizations

In this section we derive numerical approximations of the phase-field model (2.1)–(2.3) and the parametric sharp-interface model (2.13)–(2.17). Also for completeness, we include the approximation derived in [13] of the graph sharp-interface model (2.8)–(2.12).

3.1 *Phase field model*

Let $\mathcal{T}_h$ be a quasi-uniform triangulation of Ω with $h := \max_{T \in \mathcal{T}_h} \operatorname{diam}(T)$. We shall in addition assume that $\mathcal{T}_h$ is acute, i.e. that all angles of the triangles of $\mathcal{T}_h$ are $\leqslant \frac{\pi}{2}$. The finite element space S_h is defined by

$$S_h := \{\chi \in C^0(\bar{\Omega}) \mid \chi \text{ is linear on each } T \in \mathcal{T}_h\}$$

and we set

$$K_h := \{\eta \in S_h \mid |\eta(x)| \leqslant 1 \text{ for all } x \in \Omega\}.$$

We denote by $\mathcal{N}_h = \{\mathbf{x}_1, \ldots, \mathbf{x}_M\}$ the set of nodes of the triangulation and by $\{\xi_1, \ldots, \xi_M\}$ the corresponding standard basis of S_h. Finally, let $\Delta t > 0$ be a time step and $t_n = n\Delta t$, $n \geqslant 0$.

For our initial data $\varphi_h^0(\mathbf{x})$ and $u_h^0(\mathbf{x})$ we interpolate (2.4) and we discretize (2.6), (2.7) by the following method:

$$\frac{\rho}{\Delta t}(\varphi_h^{n+1} - \varphi_h^n, \eta - \varphi_h^{n+1})_h + \int_\Omega \nabla \varphi_h^n \cdot \nabla(\eta - \varphi_h^{n+1}) \geqslant \left(\frac{\varphi_h^n}{\varepsilon^2} - \frac{\pi f(u_h^n)}{4\varepsilon}, \eta - \varphi_h^{n+1}\right)_h \quad \forall\, \eta \in K_h, \tag{3.1}$$

$$\frac{\varepsilon}{\Delta t}(u_h^{n+1} - u_h^n, \chi)_h + \int_\Omega D(\varphi_h^n)\nabla u_h^{n+1} \cdot \nabla \chi + \alpha \int_{\partial\Omega} I_h(D(\varphi_h^n)(u_h^{n+1} - 1)\chi) = 0 \quad \forall\, \chi \in S_h. \tag{3.2}$$

Here, $(\eta, \chi)_h = \int_\Omega I_h(\eta\chi)$ denotes the discrete L^2 inner product and we shall also write $\|f\|_h^2 = (f, f)_h$ for the corresponding norm.

We may view ε as an approximation parameter for the sharp-interface problem and in order to resolve the interfacial region we set $h \ll \varepsilon$. Since the discretization (3.1) is explicit in time

and the only term involving φ_h^{n+1} is the lumped mass L^2 inner product it is well known that the discrete variational inequality (3.1) can be solved in the following way. First we calculate the explicit equation update $\tilde{\varphi}_h^{n+1}$ by

$$\frac{\rho}{\Delta t}(\tilde{\varphi}_h^{n+1} - \varphi_h^n, \eta)_h + \int_\Omega \nabla\varphi_h^n \cdot \nabla\eta = \left(\frac{\varphi_h^n}{\varepsilon^2} - \frac{\pi f(u_h^n)}{4\varepsilon}, \eta\right)_h \qquad \forall \eta \in S_h \tag{3.3}$$

and then we project onto K_h by setting at each node $\mathbf{x}_i$ of the triangulation,

$$\varphi_i^{n+1} = \begin{cases} -1 & \text{if} \quad \tilde{\varphi}_i^{n+1} \leqslant -1, \\ \tilde{\varphi}_i^{n+1} & \text{if} \quad -1 < \tilde{\varphi}_i^{n+1} < 1, \\ 1 & \text{if} \quad \tilde{\varphi}_i^{n+1} \geqslant 1, \end{cases} \tag{3.4}$$

where $\varphi_i^{n+1} := \varphi_h^{n+1}(\mathbf{x}_i)$ and $\tilde{\varphi}_i^{n+1} := \tilde{\varphi}_h^{n+1}(\mathbf{x}_i)$.

For simplicity of presentation we now introduce some notation. For a given node $\mathbf{x}_j$ we denote by C_j the set of nodes directly adjacent to $\mathbf{x}_j$. We split $\mathcal{N}_h$ into three sets, $\mathcal{N}_\Gamma^n$, $\mathcal{N}_+^n$ and $\mathcal{N}_-^n$, where

$$\begin{aligned} \mathcal{N}_+^n &= \{\mathbf{x}_j \in \mathcal{N}_h : \varphi_j^n = 1, \text{ and } \varphi_k^n = 1 \text{ for all nodes } \mathbf{x}_k \in C_j\}, \\ \mathcal{N}_-^n &= \{\mathbf{x}_j \in \mathcal{N}_h : \varphi_j^n = -1, \text{ and } \varphi_k^n = -1 \text{ for all nodes } \mathbf{x}_k \in C_j\}, \\ \mathcal{N}_\Gamma^n &= \mathcal{N}_h \backslash [\mathcal{N}_+^n \cup \mathcal{N}_-^n]. \end{aligned}$$

From the above definitions we see that the nodes $\mathbf{x}_j \in \mathcal{N}_\Gamma^n$ are situated in a discrete approximation of the inter-facial region $\Omega_\Gamma(t)$, while the nodes $\mathbf{x}_j \in \mathcal{N}_+^n$ and $\mathbf{x}_j \in \mathcal{N}_-^n$ are situated in discrete approximations of regions where $\varphi(\mathbf{x}, t) = 1$ and $\varphi(\mathbf{x}, t) = -1$ respectively.

Setting $\eta = \xi_j$ in (3.2), recalling that $D(\varphi) = \frac{2}{\pi}(1 - \varphi^2)$ and using the above notation we have

$$u_j^{n+1} = u_j^n \quad \forall\, \mathbf{x}_j \in \mathcal{N}_+^n \cup \mathcal{N}_-^n, \tag{3.5}$$

and hence we only need to solve (3.2) for all $\mathbf{x}_j \in \mathcal{N}_\Gamma^n$. Similarly setting $\eta = \xi_j$ in (3.3) it follows that

$$\begin{aligned} \tilde{\varphi}_j^{n+1} &= 1 + \frac{\Delta t}{\rho\varepsilon^2}\left(1 - \frac{\pi}{4}\varepsilon f(u_j^n)\right) \quad \forall\, \mathbf{x}_j \in \mathcal{N}_+^n \\ \tilde{\varphi}_j^{n+1} &= -1 - \frac{\Delta t}{\rho\varepsilon^2}\left(1 + \frac{\pi}{4}\varepsilon f(u_j^n)\right) \quad \forall\, \mathbf{x}_j \in \mathcal{N}_-^n. \end{aligned}$$

Choosing ε sufficiently small such that $1 \geqslant \frac{\pi}{4}\varepsilon \max_{[0,1]} f$ (note that $0 \leqslant u_j^n \leqslant 1$, see Section 4) from (3.4) we conclude

$$\left.\begin{aligned} \tilde{\varphi}_j^{n+1} &\leqslant -1 \quad \text{if } \varphi_j^n = -1 \\ \tilde{\varphi}_j^{n+1} &\geqslant 1 \quad \text{if } \varphi_j^n = 1 \end{aligned}\right\} \Rightarrow \varphi_j^{n+1} = \varphi_j^n \quad \forall\, \mathbf{x}_j \in \mathcal{N}_+^n \cup \mathcal{N}_-^n.$$

Thus we only need to solve (3.1) for all $\mathbf{x}_j \in \mathcal{N}_\Gamma^n$. On the other hand, if the interface always moves to the right of the domain and the initial concentration is zero everywhere, we note that $f(u_j^n) = f(u_j^0) = f(0) = 0$ for $\mathcal{N}_+^n$, so that the assumption about the smallness of ε would not be necessary.

3.2 *Sharp interface*

We now introduce approximations of the sharp-interface DIGM models (2.8)–(2.17).

3.2.1 *Graph approach.* Taking into account our rescaling of the model from Section 5.4 of [13], we see that (2.8)–(2.12) can be discretized in space using a uniform mesh size h and time step Δt, to give the following difference scheme for $j = 1, \ldots, J-1$:

$$\frac{\rho h \partial Y_j^{n+1}}{2}\left(\frac{1}{q_j^n} + \frac{1}{q_{j+1}^n}\right) = \frac{1}{hq_{j+1}^n}(Y_{j+1}^{n+1} - Y_j^{n+1}) - \frac{1}{hq_j^n}(Y_j^{n+1} - Y_{j-1}^{n+1}) + hf(U_j^n), \tag{3.6}$$

$$\begin{aligned}\frac{h\varepsilon_1(q_{j+1}^{n+1} + q_j^{n+1})\partial U_j^{n+1}}{2} &= \frac{(U_{j+1}^{n+1} - U_j^{n+1})}{hq_{j+1}^{n+1}} - \frac{(U_j^{n+1} - U_{j-1}^{n+1})}{hq_j^{n+1}} + h\varepsilon_2 \partial Y_j^{n+1} U_j^n f(U_j^n) \\ &\quad - h\partial Y_j^{n+1} U_j^n \left(1 + \frac{\rho\varepsilon_2 \partial Y_j^{n+1}}{2}\left(\frac{1}{q_j^{n+1}} + \frac{1}{q_{j+1}^{n+1}}\right)\right),\end{aligned} \tag{3.7}$$

where J is such that $2H = Jh$, $\partial U_j^{n+1} = (U_j^{n+1} - U_j^n)/\Delta t$, $\partial Y_j^{n+1} = (Y_j^{n+1} - Y_j^n)/\Delta t$ and

$$q_j^n = \left(1 + \left(\frac{Y_j^n - Y_{j-1}^n}{h}\right)^2\right)^{1/2} \quad \forall\, j \in [1, J]. \tag{3.8}$$

The boundary data and the initial data are approximated by

$$\frac{\rho h}{2\Delta t q_1^n}(Y_0^{n+1} - Y_0^n) = \frac{q_1^n}{h}(Y_1^{n+1} - Y_0^{n+1}) + \frac{h}{2} f(U_0^n), \tag{3.9}$$

$$\frac{\rho h}{2\Delta t q_J^n}(Y_J^{n+1} - Y_J^n) = \frac{1}{hq_J^n}(Y_{J-1}^{n+1} - Y_J^{n+1}) + \frac{h}{2} f(U_J^n), \tag{3.10}$$

$$U_0^n = U_J^n = 1, \tag{3.11}$$

$$Y_j^0 = 0, \quad U_j^0 = 0, \quad \forall\, j \in [0, J]. \tag{3.12}$$

We solve the tridiagonal system (3.6)–(3.12) using a direct approach to obtain values of $Y_h^{n+1}(x)$ and then from (3.8) values of $q_h^{n+1}(x)$. We then use these values of $Y_h^{n+1}(x)$ and $q_h^{n+1}(x)$ to directly solve the tridiagonal system (3.7).

3.2.2 *Parametric approach.* Setting $f(\mathbf{X}) = f(U)$ in Section 2.2 of [13] which uses techniques first introduced by Dziuk in [9], we see that (2.14) can be discretized in space using mass lumping to give the following difference scheme for $j = 1, \ldots, M-1$:

$$\begin{aligned}\frac{\rho}{2\Delta t}((h_{j+1}^n)^2 + (h_j^n)^2)(\mathbf{X}_j^{n+1} - \mathbf{X}_j^n) &= \mathbf{X}_{j+1}^{n+1} - 2\mathbf{X}_j^{n+1} + \mathbf{X}_{j-1}^{n+1} \\ &\quad + \frac{h_{j+1}^n}{2}((\mathbf{X}_{j+1}^n)^\perp - (\mathbf{X}_j^n)^\perp) f(U_j^n) + \frac{h_j^n}{2}((\mathbf{X}_j^n)^\perp - (\mathbf{X}_{j-1}^n)^\perp) f(U_j^n),\end{aligned} \tag{3.13}$$

where $h_j^n = |\mathbf{X}_j^n - \mathbf{X}_{j-1}^n|$. Here $\mathbf{X}_j^n = \mathbf{X}(s_j, t)$, for all $t \in [n\Delta t, (n+1)\Delta t)$, $j = 0, \dots, M$ is the discrete solution and each $\mathbf{X}_j = (x_j, y_j)$ is a vector in $\mathbb{R}^2$. Similarly we see that (2.15) can be written as, for any $j \in [1, M-1]$,

$$\frac{\varepsilon_1}{2\Delta t}(U_j^{n+1} - U_j^n)(h_{j+1}^n + h_j^n) = \frac{U_{j+1}^{n+1} - U_j^{n+1}}{h_{j+1}^{n+1}} - \frac{U_j^{n+1} - U_{j-1}^{n+1}}{h_j^{n+1}} - \frac{V_j^n U_j^n}{2} - \frac{\varepsilon_2 V_j^n U_j^n}{2}\left(\frac{\rho V_j^n}{|\mathbf{X}_{j+1}^n - \mathbf{X}_{j-1}^n|} - f(U_j^n)\right) \tag{3.14}$$

where

$$V_j^n = \left\langle \frac{\mathbf{X}_j^{n+1} - \mathbf{X}_j^n}{\Delta t}, (\mathbf{X}_{j+1}^n)^\perp - (\mathbf{X}_{j-1}^n)^\perp \right\rangle = -\frac{x_j^{n+1} - x_j^n}{\Delta t}(y_{j+1}^n - y_{j-1}^n) + \frac{y_j^{n+1} - y_j^n}{\Delta t}(x_{j+1}^n - x_{j-1}^n).$$

In order to evaluate boundary data that satisfies (2.17) we follow the techniques introduced in [8] yielding

$$x_0^{n+1} = -H, \quad x_M^{n+1} = H, \tag{3.15}$$

$$\frac{\rho}{2\Delta t}(h_1^n)^2(y_0^{n+1} - y_0^n) = (y_1^{n+1} - y_0^{n+1}) + \frac{h_1^n}{2}((x_1^n)^\perp - (x_0^n)^\perp) f(U_0^n) \tag{3.16}$$

$$\frac{\rho}{2H\Delta t}(h_M^n)^2(y_M^{n+1} - y_M^n) = (y_{M-1}^{n+1} - y_M^{n+1}) + \frac{h_M^n}{2}((x_M^n)^\perp - (x_{M-1}^n)^\perp) f(U_{M-1}^n). \tag{3.17}$$

For boundary data for U_h^n we set

$$U_0^n = U_M^n = 1. \tag{3.18}$$

Finally, using (2.16) we impose the following initial conditions:

$$\mathbf{X}_j^0 = (H(jh - 1), 0), \qquad U_j^0 = 0 \quad \text{for } j \in [0, M], \tag{3.19}$$

where $h = 2H/(M-1)$. We solve the three tridiagonal systems in (3.13)–(3.19) using the direct approach described for the graph model in Section 3.2.1.

4. Convergence

The aim of this section is to prove a convergence result for the numerical algorithm (3.1), (3.2). In what follows we make the additional assumption that $f(u) = u$ because we are at present not able to handle a nonlinear dependence on u. In order to simplify the presentation we introduce the following notation:

$$\varphi_h(t) := \frac{t - t_n}{\Delta t}\varphi_h^{n+1} + \frac{t_{n+1} - t}{\Delta t}\varphi_h^n, \quad t \in (t_n, t_{n+1}]$$
$$\varphi_h^+(t) := \varphi_h^{n+1}, \quad \varphi_h^-(t) := \varphi_h^n, \qquad t \in (t_n, t_{n+1}]$$

and similarly for u_h.

LEMMA 4.1 Assume that $\Delta t \leqslant \rho\gamma h^2$ for γ sufficiently small. Then

$$\sup_{0\leqslant t\leqslant T} \|\nabla\varphi_h(t)\|^2 + \int_0^T \|\varphi_{h,t}\|^2 \,\mathrm{d}t \leqslant C \tag{4.1}$$

$$\sup_{0\leqslant t\leqslant T} \|u_h(t)\|^2 + \int_0^T \int_\Omega D(\varphi_h^-)|\nabla u_h^+|^2 \,\mathrm{d}t \leqslant C \tag{4.2}$$

$$\int_0^T \|\nabla(\varphi_h^+ - \varphi_h^-)\|^2 \,\mathrm{d}t + \int_0^T \|u_h^+ - u_h^-\|^2 \,\mathrm{d}t \leqslant C\Delta t \tag{4.3}$$

$$0 \leqslant u_h \leqslant 1 \qquad \text{in} \quad \Omega \times (0,T). \tag{4.4}$$

Proof. Using $\chi = u_h^{n+1} - 1$ in (3.2) yields

$$\frac{\epsilon}{\Delta t}(u_h^{n+1} - u_h^n, u_h^{n+1} - 1)_h + \int_\Omega D(\varphi_h^n)|\nabla u_h^{n+1}|^2 + \alpha \int_{\partial\Omega} I_h(D(\varphi_h^n)(u_h^{n+1} - 1)^2) = 0.$$

Observing that $(u_h^{n+1} - u_h^n)(u_h^{n+1} - 1) = \frac{1}{2}((u_h^{n+1} - 1)^2 - (u_h^n - 1)^2 + (u_h^{n+1} - u_h^n)^2)$ we obtain after multiplying by $2\Delta t$ and summing from $n = 0, \ldots, N-1$ that

$$\epsilon\|u_h^N - 1\|_h^2 + \epsilon \sum_{n=0}^{N-1} \|u_h^{n+1} - u_h^n\|_h^2 + 2\Delta t \sum_{n=0}^{N-1} \int_\Omega D(\varphi_h^n)|\nabla u_h^{n+1}|^2 \leqslant \epsilon\|u_h^0 - 1\|_h^2 \leqslant C.$$

Now, (4.2) and the second part of (4.3) follow from the definitions of u_h, u_h^+, u_h^- and the elementary inequality

$$\|v_h\|^2 \leqslant \|v_h\|_h^2 \leqslant C\|v_h\|^2, \qquad v_h \in S_h. \tag{4.5}$$

Next, inserting $\eta = \varphi_h^n$ into (3.1) we derive

$$\begin{aligned}
&-\rho\Delta t \left\| \frac{\varphi_h^{n+1} - \varphi_h^n}{\Delta t} \right\|_h^2 - \frac{1}{2}\|\nabla\varphi_h^{n+1}\|^2 + \frac{1}{2}\|\nabla\varphi_h^n\|^2 + \frac{1}{2}\|\nabla(\varphi_h^{n+1} - \varphi_h^n)\|^2 \\
&\quad \geqslant \frac{1}{2\epsilon^2}\|\varphi_h^n\|_h^2 - \frac{1}{2\epsilon^2}\|\varphi_h^{n+1}\|_h^2 + \frac{1}{2\epsilon^2}\|\varphi_h^{n+1} - \varphi_h^n\|_h^2 - \frac{\pi}{4\epsilon}\|u_h^n\|_h\|\varphi_h^{n+1} - \varphi_h^n\|_h \\
&\quad \geqslant \frac{1}{2\epsilon^2}\|\varphi_h^n\|_h^2 - \frac{1}{2\epsilon^2}\|\varphi_h^{n+1}\|_h^2 - \frac{\rho}{2}\Delta t \left\| \frac{\varphi_h^{n+1} - \varphi_h^n}{\Delta t} \right\|_h^2 - \frac{C}{\epsilon^2\rho}\Delta t
\end{aligned}$$

by Hölder's inequality and since $\sup_n \|u_h^n\| \leqslant C$. Rearranging and applying an inverse estimate yields

$$\begin{aligned}
&\|\nabla\varphi_h^{n+1}\|^2 - \frac{1}{\epsilon^2}\|\varphi_h^{n+1}\|_h^2 + \rho\Delta t \left\| \frac{\varphi_h^{n+1} - \varphi_h^n}{\Delta t} \right\|^2 \\
&\quad \leqslant \|\nabla\varphi_h^n\|^2 - \frac{1}{\epsilon^2}\|\varphi_h^n\|_h^2 + Ch^{-2}\|\varphi_h^{n+1} - \varphi_h^n\|^2 + \frac{C}{\epsilon^2\rho}\Delta t \\
&\quad \leqslant \|\nabla\varphi_h^n\|^2 - \frac{1}{\epsilon^2}\|\varphi_h^n\|_h^2 + \frac{\rho}{2}\Delta t \left\| \frac{\varphi_h^{n+1} - \varphi_h^n}{\Delta t} \right\|^2 + \frac{C}{\epsilon^2\rho}\Delta t
\end{aligned}$$

provided $\Delta t \leqslant \gamma\rho h^2$ and γ is sufficiently small. Summation from $n = 0, \dots, N-1$ implies (4.1) and the remaining part of (4.3).

In order to prove (4.4) we use induction on n. The case $n = 0$ follows from our assumptions on u_0. Assuming that (4.4) holds for some $n \leqslant [\frac{T}{\Delta t}] - 1$, we write $u_h^{n+1} = \sum_{j=1}^M u_j^{n+1}\xi_j$ in terms of the basis functions $\xi_1, \dots, \xi_M$. Let j_0 be such that $u_{j_0}^{n+1} = \max_{1\leqslant j\leqslant M} u_j^{n+1}$. Inserting $\chi = \xi_{j_0}$ into (3.2) yields

$$\frac{\epsilon}{\Delta t}(u_{j_0}^{n+1} - u_{j_0}^n)\int_\Omega \xi_{j_0} = -\sum_{T\in\mathcal{T}_h}\sum_{j=1}^M u_j^{n+1}\nabla\xi_{j|T}\cdot\nabla\xi_{j_0|T}\int_\Omega D(\xi_h^n) + \alpha(1-u_{j_0}^{n+1})D(\xi_{j_0}^n)\int_{\partial\Omega}\xi_{j_0}. \tag{4.6}$$

Since $\mathcal{T}_h$ is non-negative, we have $\nabla\xi_{j|T}\cdot\nabla\xi_{i|T} \leqslant 0$ for $i \neq j$ which implies

$$\sum_{j=1}^M u_j^{n+1}\nabla\xi_{j|T}\cdot\nabla\xi_{j_0|T} \geqslant u_{j_0}^{n+1}\sum_{j=1}^M \nabla\xi_{j|T}\cdot\nabla\xi_{j_0|T} = 0,$$

because $\sum_{j=1}^M \xi_j \equiv 1$ in Ω. Returning to (4.6) we deduce

$$\frac{\epsilon}{\Delta t}(u_{j_0}^{n+1} - u_{j_0}^n)\int_\Omega \xi_{j_0} \leqslant \alpha(1-u_{j_0}^{n+1})D(\xi_{j_0}^n)\int_{\partial\Omega}\xi_{j_0}.$$

If we assume that $u_{j_0}^{n+1} > 1$, the above inequality would imply that $u_{j_0}^{n+1} - u_{j_0}^n \leqslant 0$ and therefore $u_{j_0}^n > 1$, a contradiction to our induction hypothesis. Thus $u_h^{n+1} \leqslant 1$ in Ω and a similar argument shows that $u_h^{n+1} \geqslant 0$ in Ω. □

As a consequence we also obtain a bound on $u_{h,t}$.

LEMMA 4.2

$$\int_0^T \|u_{h,t}\|^2_{(H^1(\Omega))'}\,\mathrm{d}t \leqslant C.$$

Proof. Let $\zeta \in H^1(\Omega)$ and $\hat{Q}_h\zeta \in S_h$ its L^2 projection with respect to $(.,.)_h$, i.e.

$$\int_\Omega \zeta v_h = (\hat{Q}_h\zeta, v_h)_h \qquad \text{for all } v_h \in S_h.$$

It can be shown (e.g. [1]) that $\|\hat{Q}_h\zeta\|_{H^1} \leqslant C\|\zeta\|_{H^1}$ for all $\zeta \in H^1(\Omega)$. Using (3.2) we obtain

$$\begin{aligned}\epsilon\left\langle\frac{u_h^{n+1}-u_h^n}{\Delta t},\zeta\right\rangle_{(H^1)',H^1} &= \epsilon\int_\Omega \frac{u_h^{n+1}-u_h^n}{\Delta t}\zeta = \epsilon\left(\frac{u_h^{n+1}-u_h^n}{\Delta t},\hat{Q}_h\zeta\right)_h\\ &= -\int_\Omega D(\varphi_h^n)\nabla u_h^{n+1}\cdot\nabla\hat{Q}_h\zeta - \alpha\int_{\partial\Omega} I_h(D(\varphi_h^n)(u_h^{n+1}-1)\hat{Q}_h\zeta)\\ &\leqslant \left\|\sqrt{D(\varphi_h^n)}\nabla u_h^{n+1}\right\|\|\nabla\hat{Q}_h\zeta\| + C\|\hat{Q}_h\zeta\|_{L^1(\partial\Omega)}\end{aligned}$$

since $|u_h^{n+1}| \leqslant 1$ on $\bar{\Omega}$. In view of the continuous embedding $H^1(\Omega) \hookrightarrow L^1(\partial\Omega)$ and the stability of $\hat{Q}_h$ in $H^1(\Omega)$ we conclude

$$\epsilon\left\langle \frac{u_h^{n+1}-u_h^n}{\Delta t}, \zeta \right\rangle_{(H^1)',H^1} \leqslant C\left(\left\|\sqrt{D(\varphi_h^n)}\nabla u_h^{n+1}\right\| + 1\right)\|\zeta\|_{H^1(\Omega)} \qquad \text{for all } \zeta \in H^1(\Omega)$$

and therefore

$$\left\|\frac{u_h^{n+1}-u_h^n}{\Delta t}\right\|_{(H^1(\Omega))'} \leqslant C\left(\left\|\sqrt{D(\varphi_h^n)}\nabla u_h^{n+1}\right\| + 1\right).$$

The result now follows from (4.2) after squaring and summing from $n = 0, \ldots, N-1$. □

Lemmas 4.1 and 4.2 now immediately imply that there exists a subsequence $h \to 0$, $\Delta t \leqslant \rho\gamma h^2$ such that

$$\begin{aligned}
\varphi_h, \varphi_h^{\pm} &\rightharpoonup \varphi && \text{in} \quad L^2(0,T;H^1(\Omega))\\
\varphi_{h,t} &\rightharpoonup \varphi_t && \text{in} \quad L^2(0,T;L^2(\Omega))\\
\varphi_h, \varphi_h^{\pm} &\to \varphi && \text{in} \quad L^2(0,T;L^2(\Omega)) \text{ and a.e. in } \Omega\times(0,T)\\
u_h, u_h^{\pm} &\overset{*}{\rightharpoonup} u && \text{in} \quad L^\infty(\Omega\times(0,T))\\
u_{h,t} &\rightharpoonup u_t && \text{in} \quad L^2(0,T;(H^1(\Omega))')\\
D(\varphi_h^-)\nabla u_h^+ &\rightharpoonup F && \text{in} \quad L^2(0,T;(L^2(\Omega))^2).
\end{aligned} \tag{4.7}$$

Our first aim is to improve the convergence properties of u_h.

LEMMA 4.3 Let $v_h := D(\varphi_h)u_h$. After possibly extracting a further subsequence we have $D(\varphi)u \in L^2(0,T;H^1(\Omega))$ and

$$\begin{aligned}
v_h &\rightharpoonup D(\varphi)u \quad \text{in} \quad L^2(0,T;H^1(\Omega))\\
v_h &\to D(\varphi)u \quad \text{in} \quad L^2(0,T;L^2(\Omega)).
\end{aligned} \tag{4.8}$$

Proof. We first show that

$$\|v_h\|_{L^2(0,T;H^1(\Omega))} \leqslant C \qquad \text{uniformly in } h \text{ and } \Delta t. \tag{4.9}$$

We infer from (4.4) that

$$\int_0^T \|\nabla v_h\|^2 \leqslant C\int_0^T \|\nabla\varphi_h\|^2 + C\int_0^T\int_\Omega D(\varphi_h)^2|\nabla u_h|^2.$$

In view of (4.1), we only have to estimate the second expression. Note that for $t \in (t_n, t_{n+1})$

$$D(\varphi_h(t)) \leqslant D(\varphi_h^n) + C|\varphi_h^{n+1} - \varphi_h^n|$$

so that we can estimate in (t_n, t_{n+1}) with the help of inverse inequalities

$$\begin{aligned}
&\int_\Omega D(\varphi_h)^2|\nabla u_h|^2 \\
&\quad\leqslant C\int_\Omega D(\varphi_h^n)^2|\nabla u_h|^2 + C\int_\Omega |\varphi_h^{n+1}-\varphi_h^n|^2|\nabla u_h|^2 \\
&\quad\leqslant C\int_\Omega D(\varphi_h^n)^2|\nabla u_h^{n+1}|^2 + C\int_\Omega D(\varphi_h^n)^2|\nabla(u_h^{n+1}-u_h^n)|^2 + C\|\nabla u_h\|_{L^\infty}^2\|\varphi_h^{n+1}-\varphi_h^n\|^2 \\
&\quad\leqslant C\int_\Omega D(\varphi_h^n)|\nabla u_h^{n+1}|^2 + C\|\nabla(u_h^{n+1}-u_h^n)\|^2 + Ch^{-2}\|u_h\|_{L^\infty}^2\Delta t\int_{t_n}^{t_{n+1}}\|\varphi_{h,t}\|^2 \\
&\quad\leqslant C\int_\Omega D(\varphi_h^n)|\nabla u_h^{n+1}|^2 + Ch^{-2}\|u_h^{n+1}-u_h^n\|^2 + C\int_{t_n}^{t_{n+1}}\|\varphi_{h,t}\|^2.
\end{aligned}$$

Integration with respect to $t \in (t_n, t_{n+1})$ and summation yields in view of (4.1), (4.3) and the condition $\Delta t \leqslant Ch^2$

$$\int_0^T\int_\Omega D(\varphi_h)^2|\nabla u_h|^2 \leqslant C\int_0^T\int_\Omega D(\varphi_h^-)|\nabla u_h^+|^2 + C\Delta t$$

and therefore (4.9). This implies the first assertion in (4.8), since $D(\varphi_h) \to D(\varphi)$ a.e. and $u_h \overset{*}{\rightharpoonup} u$ in $L^\infty(\Omega\times(0,T))$. In order to prove strong convergence of (v_h) we establish a bound on $(v_{h,t})$. Fix $p > 2$ and let $\zeta \in H^{1,p}(\Omega)$. Then

$$\begin{aligned}
\langle v_{h,t}, \zeta\rangle_{(H^{1,p})',H^{1,p}} = \int_\Omega v_{h,t}\zeta &= -2\int_\Omega \varphi_h\varphi_{h,t}u_h\zeta + \int_\Omega D(\varphi_h)u_{h,t}\,\zeta \\
&\leqslant 2\|\varphi_{h,t}\|\,\|\zeta\| + \|u_{h,t}\|_{(H^1)'}\|D(\varphi_h)\zeta\|_{H^1} \\
&\leqslant 2\|\varphi_{h,t}\|\,\|\zeta\| + \|u_{h,t}\|_{(H^1)'}(\|\zeta\|_{H^1} + \|\zeta\|_{L^\infty}\|\nabla\varphi_h\|) \\
&\leqslant C\|\zeta\|_{H^{1,p}}(\|\varphi_{h,t}\| + \|u_{h,t}\|_{(H^1)'} + \|u_{h,t}\|_{(H^1)'}\|\nabla\varphi_h\|)
\end{aligned}$$

where we used the continuous embedding $H^{1,p}(\Omega) \hookrightarrow C^0(\bar\Omega)$. Recalling (4.1) and Lemma 4.2 we deduce

$$\int_0^T \|v_{h,t}\|_{(H^{1,p})'}^2 \leqslant C,$$

which combined with (4.9) and a well known compactness result yields the strong convergence of (v_h). □

Our next step is to show that the limit φ satisfies the variational inequality (2.6).

THEOREM 1 The function φ satisfies

$$\rho\int_\Omega \varphi_t(\eta-\varphi) + \int_\Omega \nabla\varphi\cdot\nabla(\eta-\varphi) \geqslant \int_\Omega\left(\frac{\varphi}{\epsilon^2} - \frac{\pi u}{4\epsilon}\right)(\eta-\varphi)$$

for all $\eta \in K$ and a.e. $t \in (0, T)$.

Proof. Let $\eta \in K$, there exists a sequence $\eta_h \in K_h$ such that $\eta_h \to \eta$ in $H^1(\Omega)$ as $h \to 0$. We have for all $\xi \in C_0^\infty(0,T)$, $\xi \geqslant 0$

$$\begin{aligned}\rho \int_0^T \xi(t)(\varphi_{h,t}, \eta_h - \varphi_h^+)_h + \int_0^T \xi(t) \int_\Omega \nabla \varphi_h^- \cdot \nabla \eta_h \\ \geqslant \frac{1}{\epsilon^2} \int_0^T \xi(t)(\varphi_h^-, \eta_h - \varphi_h^+)_h - \frac{\pi}{4\epsilon} \int_0^T \xi(t)(u_h^-, \eta_h - \varphi_h^+)_h \\ + \int_0^T \xi(t) \int_\Omega |\nabla \varphi_h^+|^2 + \int_0^T \xi(t) \int_\Omega \nabla \varphi_h^+ \cdot \nabla(\varphi_h^- - \varphi_h^+).\end{aligned}$$

Employing the well known inequality

$$\left| \int_\Omega \eta_h \chi_h - (\eta_h, \chi_h)_h \right| \leqslant Ch \|\eta_h\| \, \|\nabla \chi_h\| \qquad \eta_h, \chi_h \in S_h \tag{4.10}$$

as well as (4.7), (4.3) and the weak lower semicontinuity of the L^2 norm we obtain in the limit

$$\begin{aligned}\rho \int_0^T \xi(t) \int_\Omega \varphi_t(\eta - \varphi) + \int_0^T \xi(t) \int_\Omega \nabla \varphi \cdot \nabla \eta \\ \geqslant \frac{1}{\epsilon^2} \int_0^T \xi(t) \int_\Omega \varphi(\eta - \varphi) - \frac{\pi}{4\epsilon} \int_0^T \xi(t) \int_\Omega u(\eta - \varphi) + \int_0^T \xi(t) \int_\Omega |\nabla \varphi|^2,\end{aligned}$$

which implies the result, since $\xi \geqslant 0$ was arbitrary. □

As $u \in L^\infty(\Omega \times (0,T))$, the regularity theory for parabolic variational inequalities (see [11]) yields

$$\varphi \in L^p(0,T; W^{2,p}(\Omega)), \quad \varphi_t \in L^p(0,T; L^p(\Omega)) \qquad \text{for all } p < \infty,$$

so that standard embedding results imply that $\varphi \in C^0(\overline{\Omega \times (0,T)})$. In particular, the set $U := \{(x,t) \in \Omega \times (0,T) \mid D(\varphi)(x,t) > 0\}$ is open.

We are now in position to identify the limit F of the sequence $(D(\varphi_h^-)\nabla u_h^+)$.

LEMMA 4.4 For $i = 1, 2$ we have $u_{x_i} \in L^2_{\text{loc}}(U)$ and $F = \chi_U D(\varphi) \nabla u$ a.e. in $\Omega \times (0,T)$.

Proof. In a first step we prove that $(D(\varphi)^2 u)_{x_i} \in L^2(\Omega \times (0,T))$ and that

$$(D(\varphi)^2 u)_{x_i} = -4D(\varphi)\varphi\varphi_{x_i} u + D(\varphi) F_i, \qquad i = 1, 2. \tag{4.11}$$

To see this, we observe that for all $\zeta \in C_0^\infty(\Omega \times (0,T))$, $i = 1, 2$

$$\int_0^T \int_\Omega D(\varphi)^2 u \zeta_{x_i} = \lim_{h \to 0} \int_0^T \int_\Omega D(\varphi_h)^2 u_h \zeta_{x_i}.$$

Next, integration by parts yields

$$\begin{aligned}\int_0^T \int_\Omega D(\varphi_h)^2 u_h \zeta_{x_i} &= 4 \int_0^T \int_\Omega D(\varphi_h) \varphi_h \varphi_{h,x_i} u_h \zeta - \int_0^T \int_\Omega D(\varphi_h)^2 u_{h,x_i} \zeta \\ &= 4 \int_0^T \int_\Omega v_h \varphi_h \varphi_{h,x_i} \zeta - \int_0^T \int_\Omega D(\varphi_h) D(\varphi_h) u_{h,x_i} \zeta.\end{aligned}$$

Lemma 4.3 together with (4.7) and the dominated convergence theorem implies that $\varphi_h v_h \zeta \to \varphi D(\varphi) u\, \zeta$ in $L^2(0,T;L^2(\Omega))$ while $\nabla\varphi_h \rightharpoonup \nabla\varphi$ in $L^2(0,T;L^2(\Omega))$, so that

$$\int_0^T \int_\Omega \varphi_h v_h \varphi_{h,x_i} \zeta \to \int_0^T \int_\Omega \varphi D(\varphi) u \varphi_{x_i} \zeta \qquad \text{as } h \to 0.$$

A similar argument as in the proof of Lemma 4.3 shows that $D(\varphi_h)\nabla u_h \rightharpoonup F$ in $L^2(0,T;(L^2(\Omega))^2)$, so that

$$\int_0^T \int_\Omega D(\varphi_h) D(\varphi_h) u_{h,x_i} \zeta \to \int_0^T \int_\Omega D(\varphi) F_i \zeta \qquad \text{as } h \to 0$$

proving (4.11). This relation now allows us to identify F on the set U. To this purpose, let $\zeta \in C_0^\infty(U)$ and compute

$$\begin{aligned} \iint_U u\zeta_{x_i} &= \iint_U D(\varphi)^2 u \frac{\zeta_{x_i}}{D(\varphi)^2} \\ &= -\iint_U (D(\varphi)^2 u)_{x_i} \frac{\zeta}{D(\varphi)^2} - 4\iint_U \frac{u\varphi\varphi_{x_i}\zeta}{D(\varphi)} \\ &= -\iint_U \frac{F_i}{D(\varphi)}\zeta \end{aligned}$$

by (4.11). It remains to identify F on the complement of U. Let $\zeta \in C_0^\infty(\Omega \times (0,T))$ be arbitrary. Clearly, $D(\varphi)(1-\chi_U) = 0$ a.e. in $\Omega \times (0,T)$ so that we infer from (4.1) and (4.7)

$$\begin{aligned} \left| \int_0^T \int_\Omega D(\varphi_h^-) u^+_{h,x_i} (1-\chi_U)\zeta \right| &\leqslant \left(\int_0^T \int_\Omega D(\varphi_h^-) |\nabla u_h^+|^2 \right)^{\frac{1}{2}} \left(\int_0^T \int_\Omega D(\varphi_h^-)(1-\chi_U)\zeta^2 \right)^{\frac{1}{2}} \\ &\leqslant C \left(\int_0^T \int_\Omega |D(\varphi_h^-) - D(\varphi)|(1-\chi_U) \right)^{\frac{1}{2}} \quad \to 0, h \to 0. \end{aligned}$$

Thus,

$$\int_0^T \int_\Omega F_i (1-\chi_U)\zeta = 0 \quad \text{for all } \zeta \in C_0^\infty(\Omega \times (0,T)), i = 1,2$$

so that $F \equiv 0$ a.e. on $\Omega \times (0,T) \setminus U$. □

Finally, let us derive the equation, which is satisfied by the limit u. Choose arbitrary test functions $\zeta \in H^1(\Omega), \xi \in C_0^\infty((0,T))$. There exists a sequence $(\chi_h) \subset S_h$ such that $\chi_h \to \zeta$ in $H^1(\Omega)$. Then

$$\begin{aligned} \epsilon \int_0^T \xi(t)(u_{h,t}, \chi_h)_h + \int_0^T \xi(t) \int_\Omega D(\varphi_h^-) \nabla u_h^+ \cdot \nabla \chi_h + \alpha \int_0^T \xi(t) \int_{\partial\Omega} D(\varphi_h^-)(u_h^+ - 1)\chi_h \\ = \alpha \int_0^T \xi(t) \left(\int_{\partial\Omega} D(\varphi_h^-)(u_h^+ - 1)\chi_h - \int_{\partial\Omega} I_h(D(\varphi_h^-)(u_h^+ - 1)\chi_h) \right). \quad (4.12) \end{aligned}$$

Let us estimate the right-hand side first. Using an interpolation argument and an inverse estimate of the form $\|v_h\|_{L^2(e)} \leqslant Ch^{-\frac{1}{2}}\|v_h\|_{L^2(T)}$ for $e \subset \partial T$ we obtain

$$\begin{aligned}
&\left|\int_{\partial\Omega} I_h(D(\varphi_h^-)(u_h^+ - 1)\chi_h) - \int_{\partial\Omega} D(\varphi_h^-)(u_h^+ - 1)\chi_h\right| \\
&\quad\leqslant Ch \sum_{e\subset\partial\Omega} \|\nabla(D(\varphi_h^-)(u_h^+ - 1)\chi_h)\|_{L^1(e)} \\
&\quad\leqslant Ch \sum_{e\subset\partial\Omega} (\|\varphi_h^-\nabla\varphi_h^-(u_h^+ - 1)\chi_h\|_{L^1(e)} + \|D(\varphi_h^-)\nabla u_h^+\chi_h\|_{L^1(e)}) \\
&\qquad + Ch \sum_{e\subset\partial\Omega} \|D(\varphi_h^-)(u_h^+ - 1)\nabla\chi_h\|_{L^1(e)} \\
&\quad\leqslant Ch \sum_{e\subset\partial\Omega} \|\chi_h\|_{L^2(e)}(\|\nabla\varphi_h^-\|_{L^2(e)} + \|D(\varphi_h^-)\nabla u_h^+\|_{L^2(e)}) \\
&\qquad + Ch \sum_{e\subset\partial\Omega} \|\nabla\chi_h\|_{L^2(e)}\|D(\varphi_h^-)(u_h^+ - 1)\|_{L^2(e)} \\
&\quad\leqslant C\sqrt{h}\|\chi_h\|_{L^2(\partial\Omega)} \left(\sum_{T\cap\partial\Omega\neq\emptyset} \|\nabla\varphi_h^-\|^2_{L^2(T)} + \|D(\varphi_h^-)\nabla u_h^+\|^2_{L^2(T)}\right)^{\frac{1}{2}} \\
&\qquad + C\sqrt{h}\|D(\varphi_h^-)(u_h^+ - 1)\|_{L^2(\partial\Omega)} \left(\sum_{T\cap\partial\Omega\neq\emptyset} \|\nabla\chi_h\|^2_{L^2(T)}\right)^{\frac{1}{2}} \\
&\quad\leqslant C\sqrt{h}\|\chi_h\|_{H^1}(\|\nabla\varphi_h^-\| + \|D(\varphi_h^-)\nabla u_h^+\| + \|D(\varphi_h^-)(u_h^+ - 1)\|_{L^2(\partial\Omega)}).
\end{aligned}$$

Thus, (4.1) and (4.2) imply that the right-hand side of (4.12) tends to zero. Passing to the limit $h \to 0$ on the left-hand side of (4.12) yields in view of (4.10), (4.7), Lemmas 4.3 and 4.4

$$\epsilon \int_0^T \xi(t)\langle u_t, \zeta\rangle_{(H^1)',H^1} + \iint_{\{D(\varphi)>0\}} \xi(t)D(\varphi)\nabla u\cdot\nabla\zeta + \alpha\int_0^T \xi(t)\int_{\partial\Omega} D(\varphi)(u-1)\zeta = 0.$$

5. Numerical results

In this section we compare phase field numerical simulations with sharp-interface ones. We also compare travelling wave speeds explicitly calculated in [6] with travelling wave speeds calculated numerically using the sharp-interface discretizations in Sections 3.2.1 and 3.2.2 of (1.5), (1.6). We note that the results in [6] are obtained using the sharp-interface model (1.3), (1.4) with $f(u) = u^2$. Also, we would ideally like to set $\varepsilon_1 = \varepsilon_2 = 0$ in our discretizations of (1.5), (1.6). However, for certain parameter values ρ and H the computations become unstable in a way which suggests that there may not be global existence for the initial-value problem (1.5), (1.6). Instead we set $\varepsilon_1 = \varepsilon$ (the phase field parameter) and $\varepsilon_2 = 0$ and since the $\varepsilon_1 u_t$ term is redundant for travelling wave solutions this should make for a good comparison. Throughout this section for any sequence $f^n \in S_h$ we set $f_h(\mathbf{x}, t) = f_h^n(\mathbf{x})$ for all $t \in [n\Delta t, (n+1)\Delta t)$. The phase field results are computed using a uniform grid $\Omega_h = (0, L) \times (-H, H)$, with mesh size h. In all the computations presented here $f(u) = u^2$. However, very similar results were obtained with $f(u) = u$.

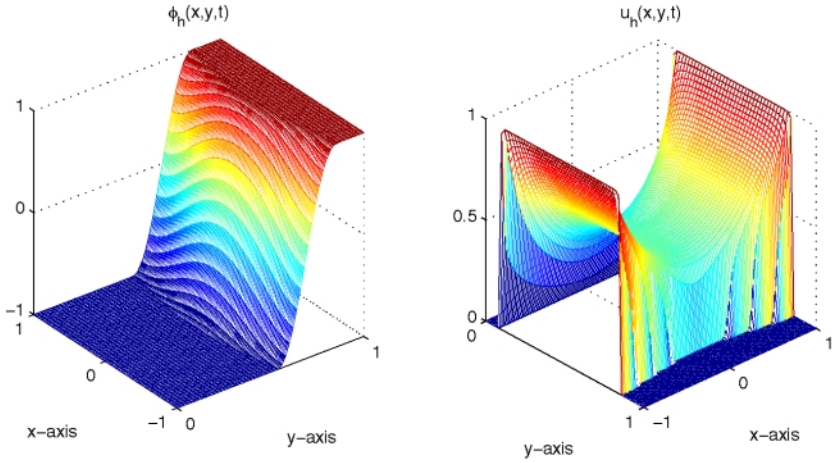

FIG. 2. The phase field solution φ_h and u_h.

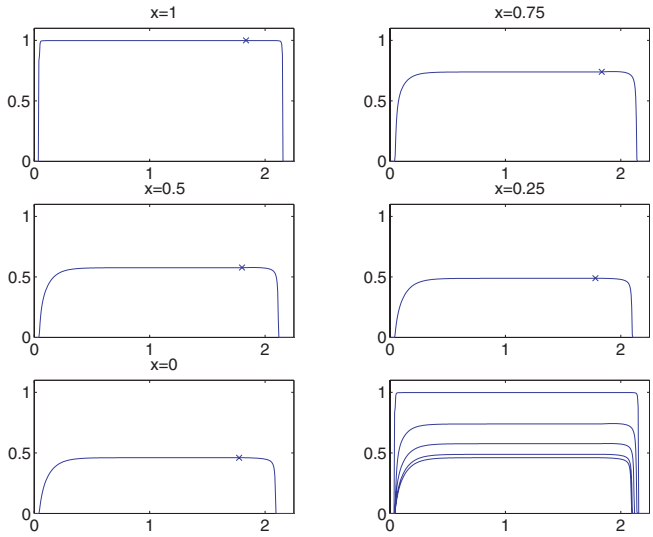

FIG. 3. Plots of the profile of u_h against y.

5.1 *Phase field computations*

In Fig. 2 we display examples of approximate phase field solutions φ_h and u_h at time $t = 0.25$. From the figure we see that the function φ_h keeps its sinusoidal shape, and that the interfacial region has width $\approx 0.3 \approx \pi\varepsilon$ and is moving in the positive y direction. The concentration u_h, which is initially identically zero, now has non-zero values in the region through which the interface has passed. In Fig. 3 we display plots of the profile of the approximate phase field solution $u_h(\cdot, y, t)$ for $t = 0.745$ and $x = 1, 0.75, 0.5, 0.25$ and $x = 0$. On each profile we plot a cross where the interfacial region begins. This enables us to see that the concentration behind the grain boundary is almost constant

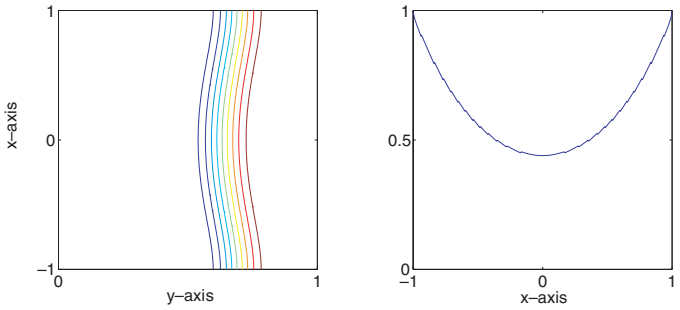

FIG. 4. A contour plot of φ_h and a plot of the averaged function $\tilde{u}_h$.

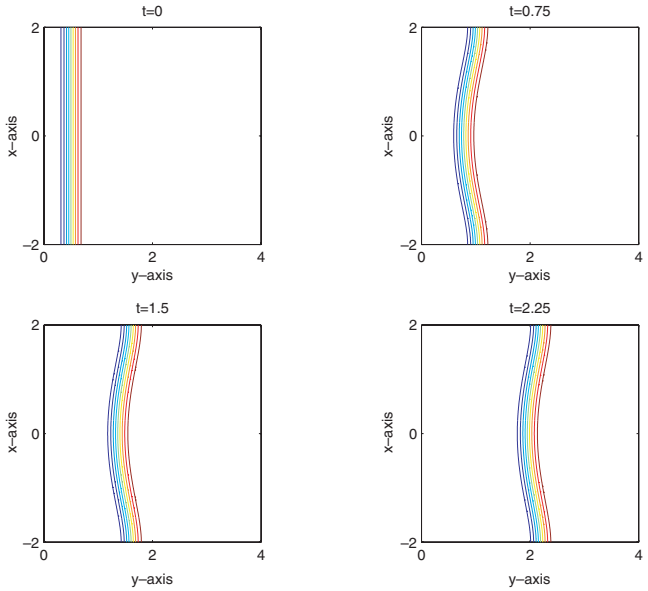

FIG. 5. The phase field solution φ_h evolving in time ($f(u) = u^2$).

in y while it drops sharply to zero at the front of the transition layer (the bottom right-hand subplot displays the five profiles together). In both computations we set $\varepsilon = 0.1, h = \frac{1}{200}, \Delta t = \frac{h^2}{40}, H = 1$, $\rho = 0.2$ and $\alpha = 1000$.

5.2 *Phase field versus sharp interface*

In Figs 5–10 we compare phase field simulations with sharp-interface ones. In order to make easy comparisons between the two solutions we display our phase field results in the form shown in Fig. 4: a contour plot of φ_h and a plot of the function $\tilde{u}_h(x, t)$ which is obtained by averaging $u_h(x, y, t)$ across the interface, i.e. over all $y : |\varphi_h(x, y, t)| < 1$. When displaying the sharp-interface simulations we always plot the graph and parametric solutions together on the same figure; for each solution we plot a cross at every 20th node of the discretization. However, in most cases

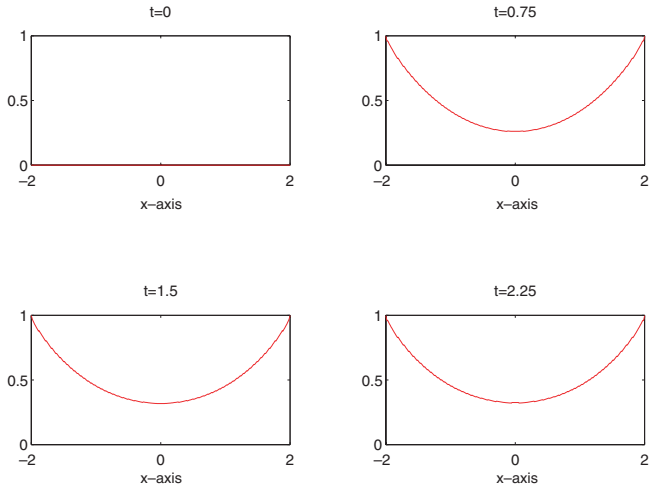

FIG. 6. The phase field solution $\tilde{u}_h$ evolving in time ($f(u) = u^2$).

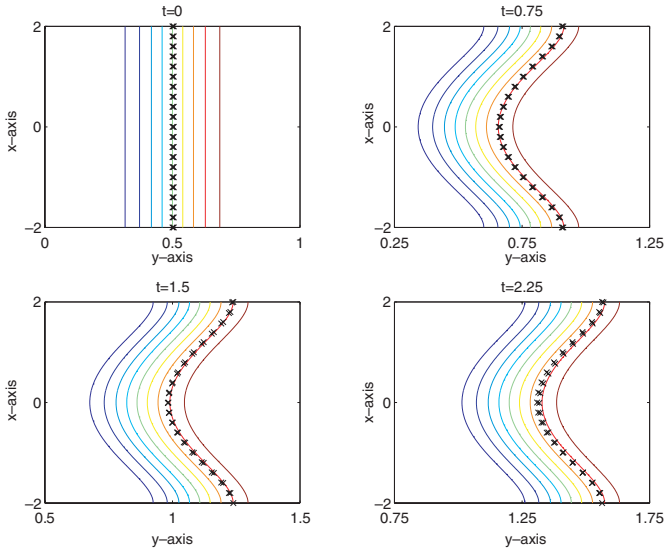

FIG. 7. Evolutionary solutions ($f(u) = u^2$, $\varepsilon_1 = \varepsilon_2 = \varepsilon = 0.2$).

only one set of crosses can be seen since on the scales shown the two solutions are effectively identical. We display two sets of results: the first set, Figs 5–8, show the evolution of an initially straight grain boundary moving along the film Ω in the positive y direction, while the second set, Figs 9 and 10, compare travelling wave solutions obtained by varying the parameters ρ and H.

5.2.1 *Evolutionary results.* For our evolutionary results we display four figures: the first two, Figs 5 and 6, show the approximate phase field solutions φ_h and $\tilde{u}_h$ respectively, while the second

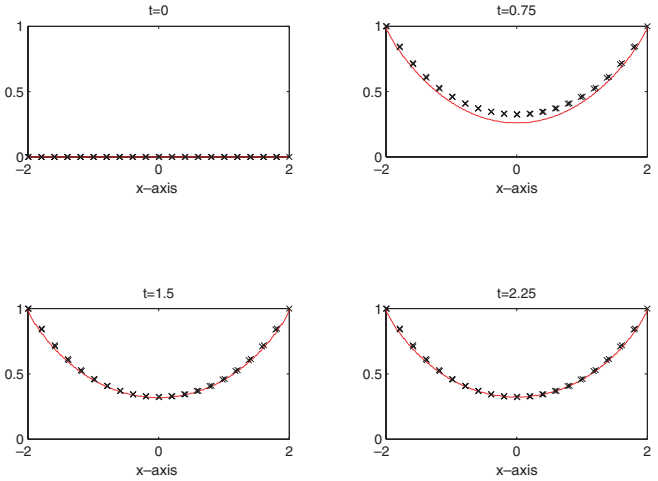

FIG. 8. Evolutionary solutions ($f(u) = u^2,\ \varepsilon_1 = \varepsilon_2 = \varepsilon = 0.2$).

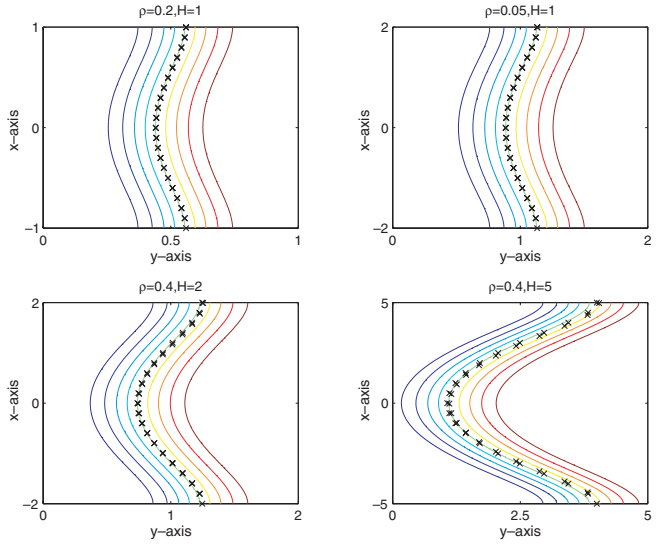

FIG. 9. Travelling wave solutions ($f(u) = u^2,\ \varepsilon_1 = \varepsilon,\ \varepsilon_2 = 0$).

two, Figs 7 and 8, show approximate sharp-interface solutions. Each figure contains four subplots that show the approximate solutions (either the grain boundary or the concentration) at times $t = 0$, $t = 0.75$, $t = 1.5$ and $t = 2.25$. In all simulations we set $h = 1/100$, $k = h^2/40$, $\rho = 0.4$ and $H = 2$ together with $\varepsilon = 0.2$ for the phase field and $\varepsilon_1 = \varepsilon_2 = 0.2$ for the sharp interface.

5.2.2 *Travelling wave solutions.* In [10] existence results for travelling wave solutions of (1.3), (1.4) are obtained, see also [13]. For our travelling wave solutions we display two figures, Figs 9 and 10, that show phase field and sharp-interface approximate solutions plotted together. Each figure

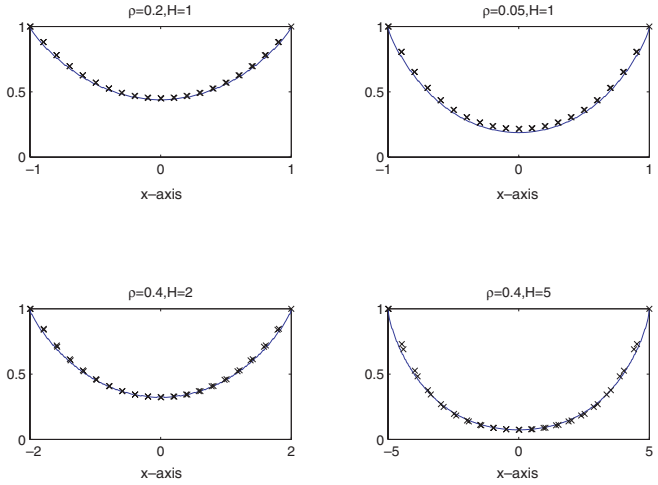

FIG. 10. Travelling wave solutions ($f(u) = u^2$ $\varepsilon_1 = \varepsilon,\ \varepsilon_2 = 0$).

contains four subplots that show the approximate travelling wave solution obtained using the values of ρ and H given at the top of the plot. We note that in Fig. 9 it is the shape of the interfacial regions that we wish to compare and not their positions. Thus we have set the nodal values where the sharp-interface solutions meet the boundaries $x = -H$ and $x = H$ to coincide with the mesh points where the minimum value of the phase field order parameter meets these boundaries. In our computations we numerically calculate the speeds of the sharp-interface graph and parametric interfacial regions by using

$$c_g^n = \frac{1}{J}\sum_{i=1}^{J} \frac{Y_i^n - Y_i^{n-1}}{\Delta t}, \quad c_p^n = \frac{1}{J}\sum_{i=1}^{J} \frac{y_i^n - y_i^{n-1}}{\Delta t}. \tag{5.1}$$

Since we are working on a uniform grid with nodes $\{ij\} : 1 \leqslant i \leqslant I, 1 \leqslant j \leqslant J$ ($I = L/h$ and $J = 2H/h$) we set for the phase field approximation φ_h, a travelling wave speed,

$$c_{pf}^n = \frac{1}{J}\sum_{i=1}^{J} \frac{\mathcal{C}_i^n - \mathcal{C}_i^{n-n_1}}{\Delta t}, \tag{5.2}$$

where $\mathcal{C}_i^n$ is the value of the y-coordinate of Ω at which $\min_{j\in J} |\varphi_{ij}^n|$ occurs and n_1 is a suitably chosen number so that $\mathcal{C}_i^n - \mathcal{C}_i^{n-n_1} \neq 0$. We say that a travelling wave solution is attained when the above speeds converge to within a given tolerence, tol $< 10^{-6}$. In Table 1 we display the values of h, Δt, ε and n_1 that are used in the four travelling wave computations shown in Figs 9 and 10. For the sharp interface computations we set $\varepsilon_1 = \varepsilon$ and $\varepsilon_2 = 0$.

5.3 *Speed of travelling wave solutions*

In Table 2 we compare travelling wave speeds c explicitly calculated in [6] with travelling wave speeds calculated numerically using the discrete graph and parametric speeds c_g and c_p obtained

TABLE 1
Parameters used in Figs 9 *and* 10

ρ	H	h	Δt	ε	n_1
0.2	1	0.005	$h^2/40$	0.1	10 000
0.05	1	0.005	$h^2/400$	0.1	50 000
0.4	2	0.01	$h^2/40$	0.2	50 000
0.4	5	0.025	$h^2/400$	0.5	100 000

TABLE 2
Travelling wave speeds ($h = 0.1$, $\Delta t = h^2/400$, $\varepsilon_1 = 0.01$, $\varepsilon_2 = 0$)

		Speeds		
ρ	H	c	c_g	c_p
0.0100	10.0	2.9460	2.967 85	2.969 99
0.0144	14.4	1.8210	1.829 39	1.830 78
0.0196	19.6	1.2159	1.219 62	1.220 61
0.0256	25.6	0.8598	0.861 73	0.862 51
0.0324	32.4	0.6361	0.637 21	0.637 87
0.0400	40.0	0.4886	0.489 21	0.489 84

TABLE 3
Travelling wave speeds reducing h and Δt ($= h^2/400$). $\varepsilon_1 = 0.01$, $\varepsilon_2 = 0$

			Graph speeds c_g			
ρ	H	c	$h = 0.2$	$h = 0.1$	$h = 0.05$	$h = 0.025$
0.0100	10.0	2.9460	3.033 68	2.967 85	2.951 46	2.947 37
0.0144	14.4	1.8210	1.854 51	1.829 39	1.823 11	1.821 54
0.0196	19.6	1.2159	1.230 85	1.219 62	1.216 81	1.216 10
			Parametric speeds c_p			
0.0100	10.0	2.9460	3.041 35	2.969 99	2.952 04	2.947 52
0.0144	14.4	1.8210	1.859 59	1.830 78	1.823 48	1.821 64
0.0196	19.6	1.2159	1.234 53	1.220 61	1.217 01	1.216 17

using (5.1). For these results we set $\varepsilon_1 = 0.01$, $\varepsilon_2 = 0$, $h = 0.1$ and $\Delta t = h^2/400$. In Table 3 we see the effect that decreasing h and thus Δt has on the numerical speeds c_g and c_p compared to the explicitly calculated speed c presented in [6]. Table 3 shows an h^2 rate of convergence to the speeds c calculated in [6] for both the graph and the parametric approximations. In Table 4 we compare the sharp-interface and phase field travelling wave speeds of the travelling wave solutions displayed in Figs 9 and 10 (using the parameter values shown in Table 1).

TABLE 4
Comparison of phase field and sharp interface travelling wave speeds

			speeds		
ρ	H	$\varepsilon = \varepsilon_1$	c_{pf}	c_g	c_p
0.2	1	0.1	2.026	2.062 96	2.063 43
0.05	1	0.1	4.800	4.889 83	4.891 54
0.4	2	0.2	0.798	0.797 90	0.798 20
0.4	5	0.5	0.415	0.410 73	0.410 86

REFERENCES

1. BARRETT, J. W., BLOWEY, J. F., & GARCKE, H. Finite element approximation of the Cahn–Hillard equation with degenerate mobility. *SIAM J. Numer. Anal.* **37**, (1999) 286–318.
2. BLOWEY, J. F. & ELLIOTT, C. M. In: NI, W., PELETIER, L. & VASQUEZ, J. L. (eds), *Curvature Dependent Phase Boundary Motion and Parabolic Obstacle Problems*, *PROC IMA Workshop on Degenerate Diffusion (1991)*. Springer, Berlin, IMA 47, (1993) pp. 19–60.
3. BLOWEY, J. F. & ELLIOTT, C. M. A phase field model with a double obstacle potential. In: BUTTAZZO, G. & VISINTIN, A. (eds), *Motion by Mean Curvature and Related Topics*. pp. 1–22. de Gruyter, New York (1994).
4. CAHN, J. W. & LIVINSTON, J. D. Discontinous coarsening of aligned entecoids. *Acta Metall.* **22**, (1974) 495–503.
5. CAHN, J. W., FIFE, P., & PENROSE, O. A phase-field model for diffusion-induced grain-boundary motion. *Acta Mater.* **45**, (1997) 4397–4413.
6. CAHN, J. W. & PENROSE, O. Theory of curvature and grooving effects in diffusion-induced grain-boundary motion. Preprint.
7. DECKELNICK, K. & ELLIOTT, C. M. An existence and uniqueness result for a phase-field model of diffusion-induced grain-boundary motion. *Proc. R. Soc. Edinburgh* A., to appear.
8. DECKELNICK, K. & ELLIOTT, C. M. Finite element error bounds for a curve shrinking with prescribed normal contact to a fixed boundary. *IMA J. Numer. Anal.* **18**, (1998) 635–654.
9. DZIUK, G. Convergence of a semi-discrete scheme for curve shortening flow. *Math. Models Meth. Appl. Sci.* **4**, (1994) 589–606.
10. FIFE, P., CAHN, J. W., & ELLIOTT, C. M. A free boundary model for diffusion-induced grain-boundarymotion. *Interfaces and Free Boundaries* **3**, (2001) 291–336.
11. FRIEDMAN, A. *Variational Principles and Free-Boundary Problems*. Wiley, New York (1982).
12. HANDWERKER, C. Diffusion-induced grain boundary migration in thin films. In: GUPTA, D. & HO, P. S. (eds), *Diffusion Phenomena in Thin Films and Microelectronic Materials*. pp. 245–322. Noyes Park Ridge, NJ (1988).
13. JUDEN, J. Numerical solution of forced curvature flow for curves and a model for diffusion induced grain boundary motion, D Phil Thesis, University of Sussex, (1998).
14. MAYER, U. F. & SIMONETT, G. Classical solutions for diffusion induced grain boundary boundary motion. *J. Math. Anal. Appl.* **234**, (1999) 660–674.
15. PURDY, G. R. Transformations involving interfacial diffusion. In: CAHN, R. W., HAASEN, P. & KRAMER, E. J. (eds), *Materials Science and Technology, A Comprehensive Treatment*. pp. 305–338. VCH, Weinheim, Germany (1990).
16. SUTTON, A. P. & BALLUFFI, R. W. *Interfaces in Crystalline Materials*. Oxford Science, (1995).